Available online at www.sciencedirect.com
SCIENCE DIRECT®
Journal of Contaminant Hydrology 64 (2003) 203–226
JOURNAL OF Contaminant Hydrology
www.elsevier.com/locate/jconhyd

Measurement and analysis of non-Fickian dispersion in heterogeneous porous media

Melissa Levy, Brian Berkowitz*

Department of Environmental Sciences and Energy Research, Weizmann Institute of Science, Rehovot 76100, Israel

Received 25 February 2002; received in revised form 2 September 2002; accepted 27 September 2002

Abstract

Contaminant breakthrough behavior in a variety of heterogeneous porous media was measured in laboratory experiments, and evaluated in terms of both the classical advection–dispersion equation (ADE) and the continuous time random walk (CTRW) framework. Heterogeneity can give rise to non-Fickian transport patterns, which are distinguished by "anomalous" early arrival and late time tails in breakthrough curves. Experiments were conducted in two mid-scale laboratory flow cells packed with clean, sieved sand of specified grain sizes. Three sets of experiments were performed, using a "homogeneous" packing, a randomly heterogeneous packing using sand of two grain sizes, and an exponentially correlated structure using sand of three grain sizes. Concentrations of sodium chloride tracer were monitored at the inflow reservoir and measured at the outflow reservoir. Breakthrough curves were then analyzed by comparison to fitted solutions from the ADE and CTRW formulations. In all three systems, including the "homogeneous" one, subtle yet measurable differences between Fickian and non-Fickian transport were observed. Quantitative analysis demonstrated that the CTRW theory characterized the full shape of the breakthrough curves far more effectively than the ADE.

Keywords: Contaminant transport; Random walk; Heterogeneous media

1. Introduction

Aquifers are highly complex in nature as they contain intricate heterogeneities at all scales. Groundwater flows through these systems in strongly varying velocity fields, so

* Corresponding author. Fax: +972-8-934-4124.
E-mail addresses: MLevy@icfconsulting.com (M. Levy), brian.berkowitz@weizmann.ac.il (B. Berkowitz).

0169-7722/03/$ - see front matter © 2003 Elsevier Science B.V. All rights reserved.
doi:10.1016/S0169-7722(02)00204-8

that describing contaminant movement becomes a fundamental problem. Another complication is that analysis of core samples and other characterization methods often provide only poor representation of the aquifer as a whole. Model development is thus focused on the difficulty of how to accurately predict contaminant movement without under- or over-simplifying what is and what is not known of aquifer properties.

Although there exists a basic conceptualization of contaminant "particles" moving continuously through heterogeneous porous media at varying velocities, describing this phenomenon is approached in a variety of ways. To date, the well-known advection–dispersion equation (ADE) with constant parameters is still the most commonly used method to characterize movement of a plume in an aquifer, despite its many known limitations. For one-dimensional flow, the ADE is given by

$$\frac{\partial C}{\partial t} = D\frac{\partial^2 C}{\partial x^2} - V\frac{\partial C}{\partial x} \tag{1}$$

where C is the solute concentration, D is the dispersion coefficient, V is the average fluid velocity, x is distance, and t is time. The ADE formulation holds two main assumptions: that the center of mass of the contaminant plume travels with the average ("macroscopic") fluid velocity and that the mechanical and chemical spread of the contaminant around this center of mass can be described completely by a Fickian process. In fact, these assumptions hold and yield a reasonable approximation of solute migration only under very specific conditions, e.g., a high degree of homogeneity in the hydraulic conductivity field (Berkowitz and Scher, 2001).

Although the ADE has been documented to provide reasonably accurate descriptions of contaminant migration in aquifers with relatively small degrees of heterogeneity (e.g., the Cape Cod site; Garabedian et al., 1991) and in early small-scale experiments as reviewed by Bear (1972), there are still many cases where the ADE fails to capture contaminant migration even in "homogeneous" systems. For example, the existence of preferential flow paths and non-Fickian tracer transport in "homogeneously" packed column experiments were clearly shown by Hoffman et al. (1996) and Oswald et al. (1997).

In sharp contrast to the ADE, field and laboratory analyses demonstrate that dispersivity is not constant but is dependent on the time and/or length scale of measurement (Gelhar et al., 1992). This is indicated in measurements that show early breakthrough times and long-time tails that are distinctly different from those of ADE-derived breakthrough curves. Such scale-dependent dispersion (also referred to as "anomalous" or "non-Gaussian") is what we refer to as "non-Fickian" transport. Non-Fickian behavior is often argued to be the result of heterogeneities, at all scales, that cannot be ignored.

Taking this argument into account, attempts have been made to use measurements at as high a resolution as possible to delineate aquifer properties (usually hydraulic conductivity). An aquifer formation is sectioned into blocks of, say, $\sim 10-50$ m^3, the effective hydraulic conductivity (or velocity) field is estimated for each block, and a numerical code that incorporates the ADE is then applied. However, even such detailed analyses have not been able to provide adequate representations of contaminant migration (e.g., Eggleston and Rojstaczer, 1998). This suggests that even at these relatively small scales, there still exist unresolved heterogeneities that are likely the root of the observed non-Fickian behavior.

Continuous time random walk (CTRW) theory is a general, physically based approach for quantifying transport, which does not rely on Fickian transport assumptions. The theory was first applied to electron movement in disordered semiconductors (e.g., Scher and Lax, 1973a,b) and more recently introduced in the context of geological materials (Berkowitz and Scher, 1995). The CTRW framework can account for a very wide range of non-Fickian and Fickian transport behaviors. In addition, the ADE can be derived from it under specific and well-defined conditions (Berkowitz et al., 2002). The CTRW theory was developed and applied to numerical studies of transport in fracture networks (Berkowitz and Scher, 1997), to consideration of the well known MADE tracer experiment (Berkowitz and Scher, 1998), and to the analysis of a tracer test in a fractured till (Kosakowski et al., 2001). Most relevant to this study are the tracer transport experiments in laboratory flow cells containing porous media that have been successfully modeled with the CTRW framework (Hatano and Hatano, 1998; Berkowitz et al., 2000).

Laboratory flow cells are an important tool in the study of contaminant transport in heterogeneous porous media (Silliman et al., 1998). Historically, dispersion experiments were performed in small-scale (usually cylindrical) column experiments of up to several tens of centimeters in length (and with diameters or widths of only several centimeters), as summarized by, e.g., Bear (1972). However, somewhat surprisingly, over the last four decades conclusions from these studies were subsequently applied at the field scale; clearly, column experiments of this size are severely limited in the types of heterogeneities that can be considered (if at all). Alternatively, the use of mid-scale flow cells (larger than 1 m in the direction of flow) allows a higher capability of producing heterogeneous structures with statistical properties similar to those found in nature. Use of such flow cells in controlled laboratory experiments is important in establishing approaches to, and limitations of, the application of current theories to field situations. Here experimental conditions are well defined and concentration (and other) data are much more accessible than in the field. Examples of studies employing experiments with mid-scale flow cells include the measurement of local water velocities (e.g., Glass et al., 1988) and measurement of the spatial distribution of solute concentrations in variable density flow systems (e.g., Schincariol and Schwartz, 1990), and measurements of variations in hydraulic conductivity (Barth et al., 2001). Although the use of mid-scale laboratory experiments has been increasing over the past 15 years, only a handful of such experiments have investigated contaminant breakthrough behavior (e.g., Silliman and Simpson, 1987; Schincariol and Schwartz, 1990).

One specific set of results, demonstrating non-Fickian transport due to small-scale heterogeneities, appears in mid-scale laboratory models of relatively homogeneous porous media (Silliman and Simpson, 1987). Subsequent analyses of breakthrough measurements from these experiments were conducted recently in order to compare solutions of the ADE and CTRW formulation (Berkowitz et al., 2000). Excellent correlation with CTRW solutions was demonstrated, but incomplete breakthrough measurements limited the analysis.

That most published results fail to present the full evolution of the solute concentration is a common problem. Generally speaking, it is at early and late arrival times where the subtleties, which strongly characterize the nature of the transport, are recognized. Therefore, in order to accurately distinguish Fickian from non-Fickian transport, careful

measurements of the full evolution of the contaminant, particularly at early and late breakthrough times, must be recorded and analyzed.

In this study, we examine non-Fickian transport in homogeneous and heterogeneous porous media. As stated above, experimental evidence (e.g., Berkowitz et al., 2000; Kosakowski et al., 2001) strongly suggests CTRW to be a precise and accurate tool for quantifying breakthrough behaviors, but further high-resolution measurements are needed to fully distinguish between Fickian and non-Fickian transport. The current report presents our most recent findings from mid-scale laboratory experiments. Experimentally measured contaminant breakthrough behavior in three different structures of porous media, focusing on the early and late arrival times, is presented and analyzed in terms of the CTRW and ADE frameworks.

2. Continuous time random walk (CTRW) theory

We present here a short summary of the conceptual picture associated with CTRW theory. Comprehensive explanations and a full accounting of the mathematical development associated with the CTRW theory have been presented elsewhere (e.g., Berkowitz and Scher, 1998, 2001; Margolin and Berkowitz, 2000, 2002; Berkowitz et al., 2002; Dentz and Berkowitz, in press), and will not be reproduced here. These studies also clearly demonstrate that approaches based on, e.g., multirate mass transfer models, double porosity models, and fractional derivative formulations of transport, are all in fact special, limiting cases of CTRW. An analysis similar to that given here, for laboratory-scale transport measurements, is given in Berkowitz et al. (2000). A complementary analysis, focusing on field-scale, non-Fickian transport in fractured media, is presented by Kosakowski et al. (2001). A practical ‘‘users’ guide’’ to application of CTRW theory solutions employed here is given in Berkowitz et al. (2001).

In the CTRW framework, contaminant migration in a strongly varying velocity field is envisioned as particles executing a series of ‘‘steps’’, or ‘‘transitions’’, through the formation via different paths with spatially changing velocities. The sporadic interaction of particles in high and moderate velocity paths with low velocity regions often leads to non-Fickian transport behaviors. Non-Fickian transport can arise if the encounter–range relationship between particles and the velocities produces a wide spread of different sequences in the flow paths of migrating particles.

This kind of transport can in general be represented by a joint probability density function, $\psi(\mathbf{s},t)$, which describes each particle ‘‘transition’’ over a distance and direction, $\mathbf{s}$, in time, t. Of course, particle movement occurs along continuous paths; our definition of discrete transitions here refers to a ‘‘conceptual discretization’’ of these paths, which can be made at as high or as low a resolution as desired. By coupling particle migration in space and time, such a function naturally accounts for particle transitions that extend over short and long distances, and over short and long times. Similar to any probabilistic/stochastic approach, we define $\psi(\mathbf{s},t)$ for an ensemble average over many possible realizations of the medium. As such, we assume here that the formation properties are stationary (i.e., statistical properties are the same at any location in the system), although the system itself is not homogeneous.

Identification of $\psi(\mathbf{s},t)$ lies at the basis of the CTRW theory. It can be shown that the principal characteristics of tracer plume migration patterns are dominated by the behavior of $\psi(\mathbf{s},t)$ at "large" times. In terms of CTRW theory, "large" time is in practice rather small, and is for all intents and purposes reached almost immediately (Berkowitz and Scher, 1998). A simple, yet general asymptotic form of $\psi(\mathbf{s},t)$ is the power law (algebraic) decay, whose long time behavior we can approximate as $\psi(\mathbf{s},t) \sim t^{-1-\beta}$, with the constant exponent $0<\beta<2$. Use of this ubiquitous, robust and well-studied power law decay form can lead to CTRW descriptions that span the full range of possible Fickian and non-Fickian behaviors.

In the context of the current study, we work with First Passage Time Distributions (FPTD). Tracer test measurements often consist of one-dimensional (averaged) tracer concentration breakthrough curves, as a function of time, t, at selected distances from the tracer source. The breakthrough usually refers to the plane of exiting particles, and the cumulative curve corresponds to what is known as a cumulative first passage time distribution, or CFPTD. In the CTRW formulation, the FPTD is defined as the probability per time for a tracer particle to reach the measurement plane at time t for the first time. The FPTD and CFPTD solutions are applicable to breakthrough curves in time, i.e., to contaminant distributions measured over fixed distances downstream of the point of tracer injection. In this context, we do not need to deal with the question of how to identify a full functional form of $\psi(\mathbf{s},t)$; the FPTD and CFPTD solutions are derived from the asymptotic form $\psi(\mathbf{s},t) \sim t^{-1-\beta}$, and the nature of the transport is described fundamentally by β.

The exponent β is controlled by the particle migration behavior, and therefore β is determined by the range of random velocities. Thus, β functionally describes the dispersion behavior. We stress, however, that the parameter β is fundamentally more general than the dispersion parameter in the ADE (e.g., Berkowitz et al., 2002). The very nature of the dispersion (e.g., Fickian or non-Fickian) can be characterized by the value of β and falls into three possible ranges: $\beta>2$, $1<\beta<2$ and $0<\beta<1$. For $\beta>2$, the first two (temporal) moments (mean and standard deviation) of $\psi(\mathbf{s},t)$ are finite, and the behavior of the tracer plume will be Fickian. In this case, the tracer plume center of mass, or mean location of the plume, l, travels at the average fluid velocity (and therefore scales as time t), while the standard deviation, σ, scales as $t^{1/2}$. This case is equivalent to the ADE and thus the breakthrough curves (FPTD and CFPTD solutions) are Fickian in shape.

For $1<\beta<2$, the second (temporal) moment of $\psi(\mathbf{s},t)$ is infinite, and the mean of the tracer plume moves with a constant velocity (which is for all practical purposes equal to the average fluid velocity). The curves are asymmetric with long late time tails and as β increases the resulting FPTD and CFPTD solutions become sharper and less disperse. In this case, because the mean of the transition time (i.e., the first temporal moment of $\psi(\mathbf{s},t)$) is finite, the shape of the CFPTD curves is a function of the actual spatial scale, as well as a function of β. For $0<\beta<1$, the FPTD and CFPTD curves display the most anomalous behavior. The curves are not symmetrical and long early and late time tails exist. Because the first two temporal moments of $\psi(\mathbf{s},t)$ are infinite, and the mean and standard deviation each scales as t^{β}, the shapes of the FPTD and CFPTD curves are functions of β, and are similar on different spatial scales.

3. Materials

3.1. Experimental apparatus

The experiments were conducted in two laboratory flow cells (A and B) filled with porous media. The design of the experimental flow cells is illustrated in Fig. 1. The internal dimensions of flow cells A and B are $0.86 \times 0.45 \times 0.10$ m and $2.13 \times 0.65 \times 0.10$ m, in the x-, y- and z-directions, respectively. The flow cells were designed to allow flow to be established with a mean gradient parallel to the (horizontal) x-axis of the cell. Inflow and outflow reservoirs located at each end of the flow cell were separated from the porous medium by a lattice support and a fine mesh screen with a hydraulic conductivity larger than the filling material. Constant head inflows and outflows were maintained across the medium by use of overflow (spill) flasks connected to the two reservoirs; this setup allowed flow along the x-axis of the cell.

The outflow reservoir volume was minimized to increase the accuracy of the conductivity measurements of the effluent. This is important because as tracer (see Section 4) moves into the outflow reservoir, it is diluted by the existing effluent contained in the reservoir. In order to minimize the dilution effects, spacers were positioned inside the effluent reservoir. In addition, peristaltic pumps (with flow dampeners) were operated constantly in both reservoirs to ensure that the reservoirs were well mixed. A flow-through electrical conductivity meter measured the conductivity of the effluent leaving the outflow reservoir in order to determine the effluent tracer concentration.

3.2. Experimental porous media

Three series of experiments were conducted, each with a different porous medium structure. The sands used were cleaned and sieved by UNIMIN, USA. These sands are well-rounded quartz sands with minimal surface coatings (99.8% pure SiO_2, as reported by UNIMIN). Three grain sizes were used in this study, each with a corresponding hydraulic

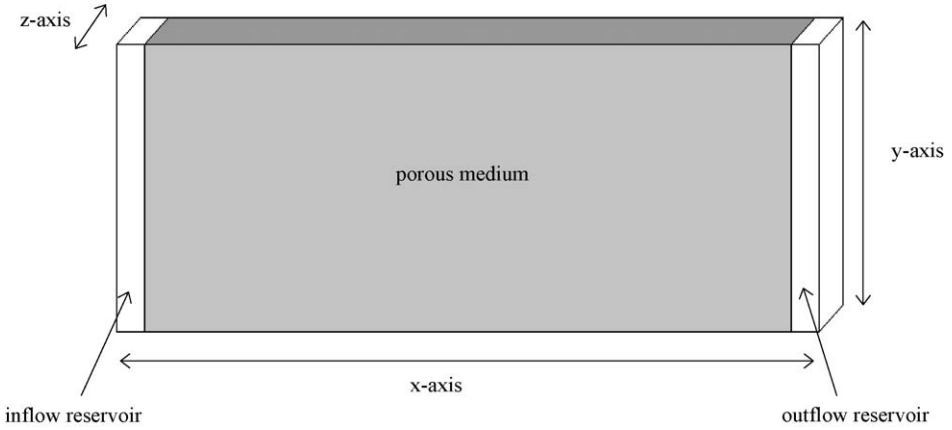

Fig. 1. Schematic representation of the experimental flow cells.

Table 1
Properties of the three sands used

	Mesh size	Grain diameter (mm)	Hydraulic conductivity (cm/s)
Sand 1	12/20	1.105	0.50
Sand 2	30/40	0.532	0.15
Sand 3	50/70	0.231	0.014

conductivity estimated from constant head column experiments (Table 1). Similar estimates were reported by Silliman and Caswell (1998), Schroth et al. (1996), and Chao and Rajaram (2000).

The first set of experiments used a uniform, "homogeneous" packing of Sand 2 in cell A, as a control. The second series of experiments, emulating Silliman and Simpson's

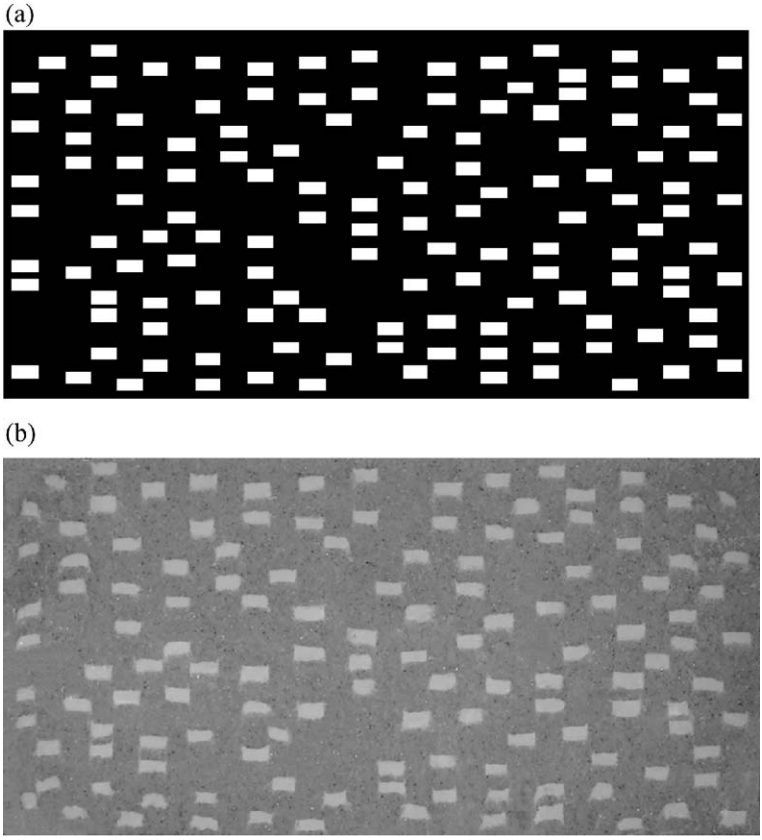

Fig. 2. (a) Computer-generated distribution of the randomly heterogeneous structure, where black and white depict high and low conductivity sands, respectively. (b) Final distribution of porous media within flow cell A (dimensions: 86 × 45 × 10 cm), as seen through the front wall. Sand 1 and Sand 3 are seen as the darker and lighter shades, respectively.

(1987) "uniform heterogeneity" structure, was also packed in cell A. A schematic diagram and a photograph of the packing of this structure are shown in Fig. 2, where the darker (black in the schematic diagram) regions represent the high conductivity sand and the light (white in the schematic diagram) regions represent the low conductivity sand. The structure was computer-generated using Matlab, producing 132 blocks (with dimensions of 6 units in the horizontal direction and 3 units in the vertical direction) distributed randomly and uniformly in a grid of 172 × 90 units. This refinement of the grid allowed the blocks to be distributed so that the occurrence of preferential path lines through the high conductivity sand was minimized. In this medium, blocks of Sand 3 (with dimensions of ~ 3 cm in the horizontal direction, 1.5 cm in the vertical direction and uniform over the 10 cm width of the flow cell) were placed within a matrix of Sand 1. The low conductivity blocks of sand occupied ~ 16% of the total volume. The objective of this set of experiments was to obtain a full evolution of the breakthrough curves in such a medium (as mentioned previously, late times were not recorded in Silliman and Simpson's, 1987 similar packing).

In the third set of experiments, all three sands were used in cell B. The computer-generated schematic along with a photograph of the packing structure is shown in Fig. 3. This heterogeneous structure functioned as a laboratory simulation of a random sedimentary structure reminiscent of some natural field sites. Using the discrete analysis random field generator (Silliman and Wright, 1991), the structure was generated as a realization of

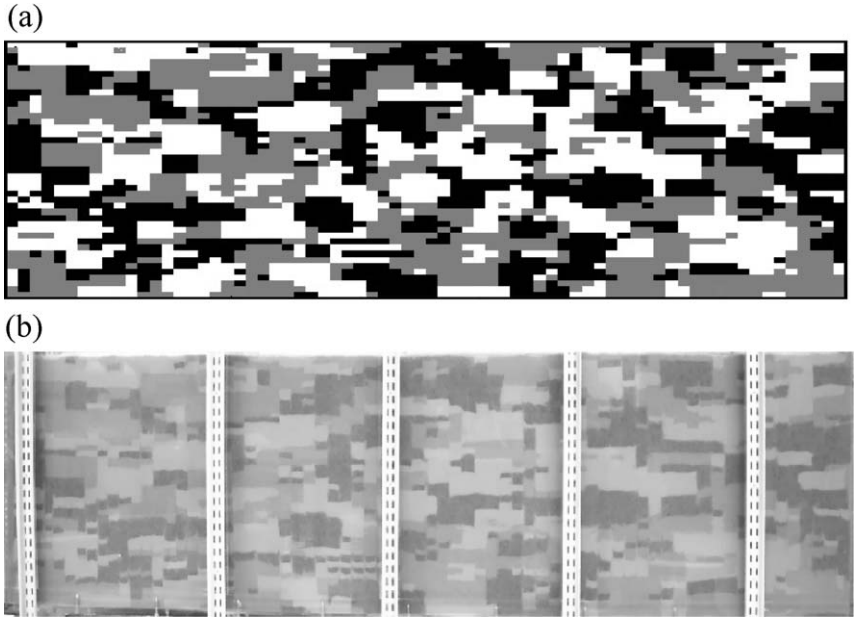

Fig. 3. (a) Computer-generated distribution of the exponentially correlated structure, where black, grey and white depict high, medium and low conductivity sands, respectively. (b) Final distribution of porous media within flow cell B (dimensions: 213 × 65 × 10 cm), as seen through the front wall. Sand 1, Sand 2 and Sand 3 are seen as the darker, intermediate and lighter shades, respectively.

a second-order stationary random field with exponential correlation. We arbitrarily chose an anisotropy ratio (x to y directions) of 2:1 for the sediment units, making each unit 3 cm along the x-axis by 1.5 cm along the y-axis. Following Silliman et al. (1998), the integral scale was selected to be four times the minimum packing dimension. Therefore, the correlation structure was approximately exponential with correlation scales of 12 cm in the x-axis and 6 cm in the y-axis, providing approximately 18×11 correlation scales within the flow cell. The medium was uniform over the z-axis. The percentages of the three sands were approximately equal (within 2%).

In all three experiments, packing of the sands was carried out under saturated conditions, with the sand being poured through at least 2 cm of water in order to avoid air entrapment. In both the second and third (heterogeneous) systems, the computer-generated packing structures were transferred to transparent sheets, to scale, and attached to the wall of the flow cell to be used as templates for packing. The sands were then added to the flow cell according to the template. The sands were packed in 1.5 cm layers using narrow metal dividers (with thickness less than 1 mm) to establish sharp contacts between regions of different conductivity sands. The dividers were removed as packing progressed. The distribution at the wall (Figs. 2b and 3b) includes slightly blurred contacts between different regions due to leakage around the metal dividers at the wall surface during packing. However, the contact between the sands in the interior of the flow cell is sharper than observed at the wall, as verified during unpacking of the flow cell.

4. Experimental procedure

Sodium chloride tracer was added to the inflow reservoir as a step change in concentration. Note that this was a continuous injection. A step input boundary condition was selected for two reasons: (i) such an inlet concentration condition is easily controlled in the experimental set-up, and (ii) breakthrough curves resulting from a step input condition are highly effective in distinguishing early and late time behavior in breakthrough curve tails (whereas a pulse input, for example, tends to be more effective when analyzing the center of mass of a plume). In all experiments, the NaCl concentration was 500 mg/l above the NaCl background concentration of the tap water. This concentration of NaCl was chosen so as to minimize density effects yet still provide a sufficiently broad range over which meaningful concentration measurements could be made (Schincariol and Schwartz, 1990; Silliman and Simpson, 1987). Provisions were made to introduce an instantaneous injection front, with little disruption of the flow field. This was accomplished by injecting a specified concentrated solution of NaCl into the inflow reservoir, creating a 500-mg/l NaCl concentration within the inflow reservoir. Simultaneously, the tubing leading to the inflow reservoir was emptied and refilled with the tracer. It is noted that this method produced a brief period of non-steady flow within the flow cell. However, monitoring the volumetric flux from the outflow reservoir indicated that the period of non-steady flow was substantially less than 1 min in all experiments and was therefore considered negligible compared to the duration of the experiments (380–10,000 min).

Several tests were carried out to ensure that experimental artifacts, such as wall effects and inlet/outlet boundary conditions, could be considered negligible. A neutral colored dye

was injected into the inlet and outlet reservoirs to ensure that the reservoirs were well mixed. In all experiments, the mixing and residence times of tracer within the reservoirs was negligible with respect to the duration of the experiments. Breakthrough of NaCl was first measured in the flow cell filled only with water, and no anomaly was observed. Breakthrough curves measured in subsequent experiments with each of the porous medium systems were reproducible for different flow rates; the measured breakthrough curves were also verified to be completely reproducible after emptying and repacking the homogeneous system. As discussed in Section 5.1, the estimated overall measurement error is considered to be much smaller than the variations in the actual measurements, and in the deviations between the measurements and the ADE-based breakthrough behavior. Finally, repeated tests with injection of the colored dye, in both the inlet and outlet reservoirs, and at injection points within the porous medium itself, did not reveal any channeling along the walls of the flow cell or along the upper and lower boundaries of the system.

The experiments were conducted at a constant room temperature of 23 °C. The concentration of the tracer was monitored at the outflow reservoir with a calibrated flow-through electrical conductivity cell. The conductivity cell was calibrated over the range of tracer concentrations used. The conductivity measurements were then converted to concentration values utilizing the calibration curves. All tracer experiments were run until the conductivity cell indicated that the concentration at the outflow reservoir was steady and equal to the inflow concentration.

Because the conductivity cell is located just after the outflow reservoir, the actual measurements taken are of the tracer after being diluted both in the outflow reservoir and in the tubing between the flow cell and the conductivity cell. Even with the outflow reservoir being minimized, there remains some inaccuracy in the measurements. In order to account for dilution in the outflow reservoir, the measured tracer concentrations, $g(t)$, were corrected to more accurately reflect the concentration of tracer just as it reaches the outflow reservoir, $f(t)$. All concentration values were corrected according to the equation

$$g'(t) = (f(t) - g(t))(F/V) \tag{2}$$

where F is the constant volumetric flow rate and V is the constant volume of the outflow reservoir. In other words, in time dt, $f(t)F$dt of tracer flows into the outlet reservoir and $g(t)F$dt of tracer flows out of the outflow reservoir. Thus, the mass flux in the outflow reservoir, $g'(t)V$, is $(f(t)-g(t))F$, leading to Eq. (2). Since discrete data were used, we estimated $g'(t)$ by $(\Delta g(t)/\Delta t)$.

Input data for the CTRW and ADE analyses consist of breakthrough curve measurements, in the form of pairs of concentration versus time values. Because we introduced the NaCl tracer as a step increase rather than as an instantaneous point injection, the concentration measurements are cumulative. We emphasize that we consider here averaged, one-dimensional concentration measurements, corresponding to one-dimensional averaged, two-dimensional flow fields of the tracer.

The CFPTD solutions can be evaluated numerically with relative ease. A series of subroutines written in the C programming language, which are evaluated within the GRACE graphical analysis package, were applied to the data. The solutions from the ADE

and CTRW formulations, along with the experimental data, were plotted and iterative fitting of the solutions to the data points was achieved. For a detailed discussion, we refer the reader to Berkowitz et al. (2001). The software and instructions for operation can be downloaded at www.weizmann.ac.il/ESER/People/Brian/CTRW.

The nonlinear curve fitting option in GRACE was used to fit the CFPTD curves to the experimental data. Initial analysis of the data sets indicated that optimal fits of the CTRW solutions could be obtained with β in the range $1<\beta<2$. As discussed in detail by Berkowitz et al. (2001), a parameter, t_{mean}, must be fit in order to translate between dimensionless units in the CFPTD solution and the dimensional temporal units of the laboratory measurements. For the CFPTD calculations, and the relevant range of β, a convenient initial estimate of t_{mean} was given by the time at which the normalized concentration is about 0.5. We were careful in testing the optimal parameter values returned by the fitting routine, due to the possible existence of multiple local minima.

A critical aspect of any model is the number of fitting parameters used in its application. In its treatment to the experiments considered here, the ADE model involves two explicit fitting parameters—the dispersion, and the average velocity. The average velocity was not estimated specifically, and was instead used as a free parameter in the ADE curve fits to the data. Moreover, application of the ADE model involves an implicit third parameter: β is not fit, it is (implicitly) prescribed ($\beta>2$). The CTRW solutions considered here require the same number of parameters. Furthermore, we note that imposition of the ADE model on a transport process assumes Fickian transport; this leads to the average tracer velocity being essentially equal to the average fluid velocity. This is also true for CFPTD curves where $\beta>1$ (Margolin and Berkowitz, 2000). In such cases, measurement of the average fluid velocity elminates one fitting parameter in both the ADE and CTRW models.

The breakthrough curves were analyzed by comparison to the fitted solutions of the ADE and CTRW formulations. In the CTRW solutions, an effort was made to obtain an optimal fit over the entire range of each data set. As noted above, the ADE solution assumes implicitly that $\beta>2$. For the ADE solutions, the central region of the breakthrough curves (where the relative concentration is near 0.5) was used as the basis for obtaining optimal fits. Careful examination of the early and late time portions of the breakthrough curves was carried out in order to distinguish between Fickian (ADE) and non-Fickian (CTRW) transport behavior.

The current investigation emphasizes the use of CTRW theory and contrasts it with the familiar ADE model. Thus, notwithstanding the fact that other parameters are involved in both the CTRW and ADE fits (essentially to relate dimensionless solutions to dimensional measurements), we focus here on the overall fit of the CTRW and ADE solutions, as characterized by, respectively, the values of β and dispersion, D. The value of β in the CTRW framework characterizes the non-Fickian nature of the transport, and the degree of "deviation" from conventional ADE solutions.

In a separate set of experiments, qualitative experiments were conducted in order to illustrate the nature of the transport and the quantitative results. Colored dye (neutral food coloring), used as a tracer, was added into the porous media as point injections. For each experiment, either five or seven pulse injection points were added along the (vertical) y-axis just past the inflow reservoir. In order to minimize density effects of the dye, salt

water, with the same density of the dye, was used as the influent throughout the entire experiment. A high-resolution digital camera was used to take photographs at various times to qualitatively illustrate the movement of the tracer plumes.

5. Results and discussion

5.1. Breakthrough curve analysis

For each experiment, accurate measurements were recorded throughout the entire evolution of the contaminant plume, including the early and late breakthrough concentrations. Breakthrough curves from all three sets of experiments were plotted on concentration (normalized) versus time graphs. The measured concentrations were normalized by the inlet step concentration. As described in Section 4, Eq. (2) was used to account for the dilution of the tracer within the outflow reservoir and in the tubing between the flow cell and the conductivity cell. Note, however, that this equation holds under the assumption that the outflow reservoir is well mixed. Because the maximum pumping rate on the pumps is 1000 ml/min, it took approximately 50 s for the entire volume to be replaced and be fully mixed in flow cell A and approximately 90 s in flow cell B. This is accounted for in the estimated measurement error. Other small but cumulative sources of error include the sensitivity of the conductivity cell, as well as the potentially small difference between the concentrations of influent inside the inflow reservoir at the initial moment of the step change and the source of tracer being pumped into the inflow reservoir. A total of approximately $\pm 0.005-0.006$ (tank A) and $\pm 0.006-0.007$ (tank B) error in the normalized concentration (y-axis) is thus estimated for each data point. The diameters of the points shown on the graphs are slightly smaller than these error estimates.

The experimental results were compared against the ADE and CTRW solutions that are shown as dashed and solid lines, respectively, in all figures. The generated solutions shown here represent "best fit" solutions. For the CTRW framework, each of the experimental breakthrough curves is fit using a separate value of β. Each ADE solution is similarly fit with a separate value for dispersion (D, from Eq. (1)). All data points were considered when fitting the curves. The CFPTD curves fit well over the complete range of measured data in all experiments and are within or close to the measurement error. In most cases, the ADE model yielded poor results, particularly in the early and/or late time regions of the curves. Only under specific conditions did the ADE characterize transport behavior well, as is presented and discussed in the next sections. The agreement of the CFPTD curves with the measurements is clear and permits differentiation between the CTRW and ADE solutions.

5.2. Homogeneous system

The experiments conducted with the homogeneous system were planned both in order to ensure correct operation of the flow cell and to act as a control. In fact, analysis of tracer migration in this flow cell revealed interesting findings in their own right. Seven experiments were run in all, at various flow rates. Three representative breakthrough

curves are shown here at the slowest, intermediate and fastest flow rates; the first with a flow rate of 36 ml/min, the second with a flow rate of 53 ml/min and the third with a flow rate of 74 ml/min. Measured breakthrough curves along with the ADE and CTRW fits are presented in Fig. 4 for all three experiments. The curves provide a contrast between the ADE (Fickian) solutions and CTRW (non-Fickian) results. In Fig. 4a, the difference between the two fits is small yet apparent at the late times. Of the three experiments, this was conducted at the slowest flow rate (36 ml/min). As the flow rate increases to 53 and to 74 ml/min, the evolving differences at the early and late breakthrough times between the ADE and CTRW solutions become more substantial (Fig. 4b,c). We emphasize that here, as well as in all other graphs below, adjustment of the ADE parameters to improve the early time fits caused, concurrently, even poorer fits to the late time data and vice versa.

These results were somewhat unexpected given the high quality and uniformity of the sand used in this packing. Although it is generally assumed that the movement of tracer in a homogeneous medium, such as this, will follow Fickian processes, our results are not the only ones that do not support these general assumptions. In fact, a number a recent studies using magnetic resonance imaging to visualize flow conditions within homogeneous geologic materials in column experiments report preferential flow paths (influencing water flow and tracer transport) (e.g., Hoffman et al., 1996; Oswald et al., 1997). These occur due to macro-structures, caused e.g. from bridging effects, and also due to micro-structures, reflecting grain-size heterogeneities.

The CFPTD curves for this set of experiments fit the measured tracer concentrations particularly well as compared to the ADE fits; this is especially so for the higher flow rate experiments. The nature of the transport behavior is also well represented in the β values that fit the breakthrough curves. Notice that as the flow rate decreases, β approaches 2 (recalling that Fickian behavior occurs for $\beta > 2$) and the shapes of the CFPTD and ADE curves become more similar. This can be explained by an interplay between slower and faster flow regions that occurs at the slower flow rates, which essentially "evens out" the tracer breakthrough concentrations. As a result, the overall transport appears more Fickian-like. At higher flow rates, there is an increasing deviation from Fickian behavior, as effects of tracer "trapped" or retarded in slower flow regions become more important. These effects are seen even more distinctly in the other two series of experiments. Further insight into the non-Fickian migration patterns in this structure is given in a qualitative demonstration in Section 5.4.

5.3. Randomly heterogeneous and exponentially correlated systems

The randomly heterogeneous structure (Fig. 2), as mentioned earlier, was chosen to emulate Silliman and Simpson's (1987) uniform heterogeneity structure, which demonstrated anomalous transport behavior, but with incomplete breakthrough measurements. In our case the characteristic late breakthrough times were also recorded in order to analyze the full evolution of the contaminant plume. It is noted that these experiments were conducted in a flow cell of approximately half the length of that used by Silliman and Simpson (1987). Ten experiments were performed at various flow rates. Three representative breakthrough curves are shown here at the slowest, intermediate and fastest flow rates; the first with a flow rate of 35 ml/min, the second with a flow rate of 47 ml/min and

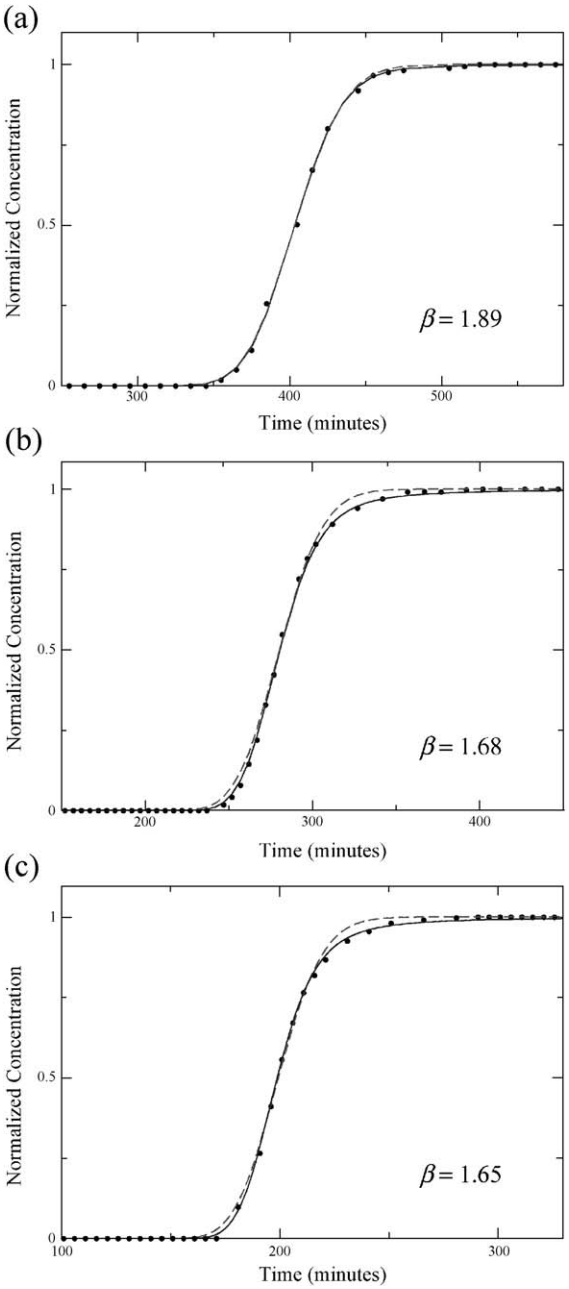

Fig. 4. Measured breakthrough curves with fitted ADE (dashed lines) and CFPTD (solid lines) solutions for the homogeneous medium. Flow rates for each experiment were (a) 36 ml/min, (b) 53 ml/min and (c) 74 ml/min. Values of β are indicated for each CFPTD fit. Corresponding values of dispersion, D, for the ADE fits are (a) 0.037, (b) 0.072 and (c) 0.120 cm^2/min.

the third with flow rate of 70 ml/min. These breakthrough curves, along with fitted solutions of the ADE and CTRW, are shown in Fig. 5.

For the third set of tracer experiments the exponentially correlated structure was used (Fig. 3). Eight experiments were carried out at various flow rates. Three representative breakthrough curves are shown here at the slowest, intermediate and fastest flow rates; the first with a flow rate of 11 ml/min, the second with a flow rate of 75 ml/min and the third with a flow rate of 175 ml/min. Breakthrough curves along with fitted ADE and CTRW solutions are displayed in Fig. 6.

Results from experiments on both of these heterogeneous structures show trends in the shapes of the breakthrough curves similar to those of the homogeneous packing experiments. Again, at the slowest flow rates, both the ADE and CFPTD curves fit the measured data well. At higher flow rates, though, the ADE solution does not fit the early and/or late breakthrough times. The CTRW framework, on the other hand, quantifies the measured data remarkably well. It is also important to note the β values for each CFPTD curve. In the first set of experiments with the homogeneous packing, the β values increase as the flow rate decreases. In the two cases where the media are explicitly heterogeneous, we see the same trend; here though, the β values are consistently lower. The values of β are smaller for the runs with faster flow rates in the randomly heterogeneous packing and the exponentially correlated structure ($\beta = 1.45$ and 1.59, respectively) than for runs with slower flow rates ($\beta = 1.71$ and 1.67, respectively). Intermediate flow rates produced breakthrough behavior with intermediate values of β ($\beta = 1.59$ and 1.64 for the randomly heterogeneous structure and the exponentially correlated structure, respectively).

The range of β values found within and among the homogeneous and heterogeneous porous medium systems is relatively narrow, because the heterogeneity patterns and differences in hydraulic conductivity among the three sands are moderate. However, the variations in β values found here do signify subtle yet important differences in the evolution of the tracer migration. Because smaller values of β are typical of more heterogeneous systems, the above results indicate that as the flow rate increases, there is less interplay between advective and diffusive transport, and thus less smoothing. At lower flow rates, transport becomes more Fickian-like due to greater interplay between advective and diffusive processes and mixing among streamlines. This is illustrated visually in Section 5.4.

The preceding analysis demonstrates also that β is velocity dependent. Recall that we base our current analysis on the general form $\psi(\mathbf{s},t) \sim t^{-1-\beta}$ for the transition time distribution: the nature of the overall transport is then embodied by β, and we therefore do not explicitly distinguish between the contributions of (slow or fast) advective and diffusive transport. Thus, because of the interplay and relative contributions between advective and diffusive transport (at different length scales), β can vary under different flow scenarios in any given heterogeneous medium. The variations in β values reported for the above experiments are entirely consistent with the CTRW theory (see Section 2 and references therein for conceptual and theoretical details).

5.4. Dye tracer experiments

Viewing distributions of a dye tracer migrating through the medium provides a qualitative picture of the flow path patterns. Fig. 7 displays a set of photographs from

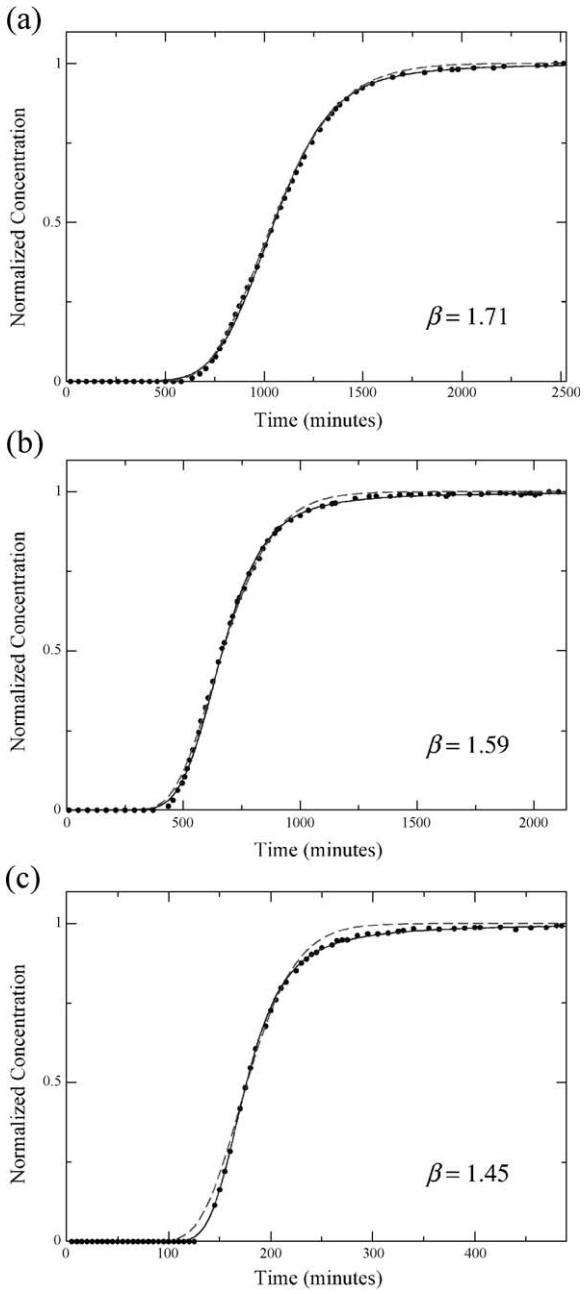

Fig. 5. Measured breakthrough curves with fitted ADE (dashed lines) and CFPTD (solid lines) solutions for the randomly heterogeneous medium. Flow rates for each experiment were (a) 35 ml/min, (b) 47 ml/min and (c) 70 ml/min. Values of β are indicated for each CFPTD fit. Corresponding values of dispersion, D, for the ADE fits are (a) 0.212, (b) 0.348 and (c) 0.898 cm^2/min.

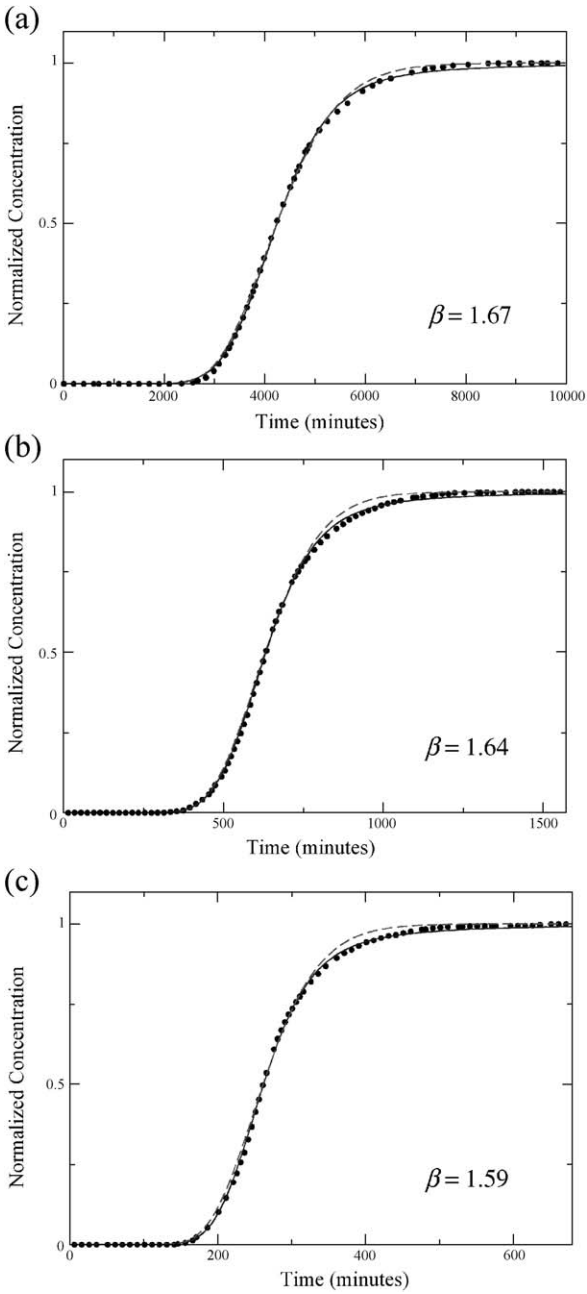

Fig. 6. Measured breakthrough curves with fitted ADE (dashed lines) and CFPTD (solid lines) solutions for the exponentially correlated medium. Flow rates for each experiment were (a) 11 ml/min, (b) 74 ml/min and (c) 175 ml/min. Values of β are indicated for each CFPTD fit. Corresponding values of dispersion, D, for the ADE fits are (a) 0.265, (b) 1.65 and (c) 4.30 cm^2/min.

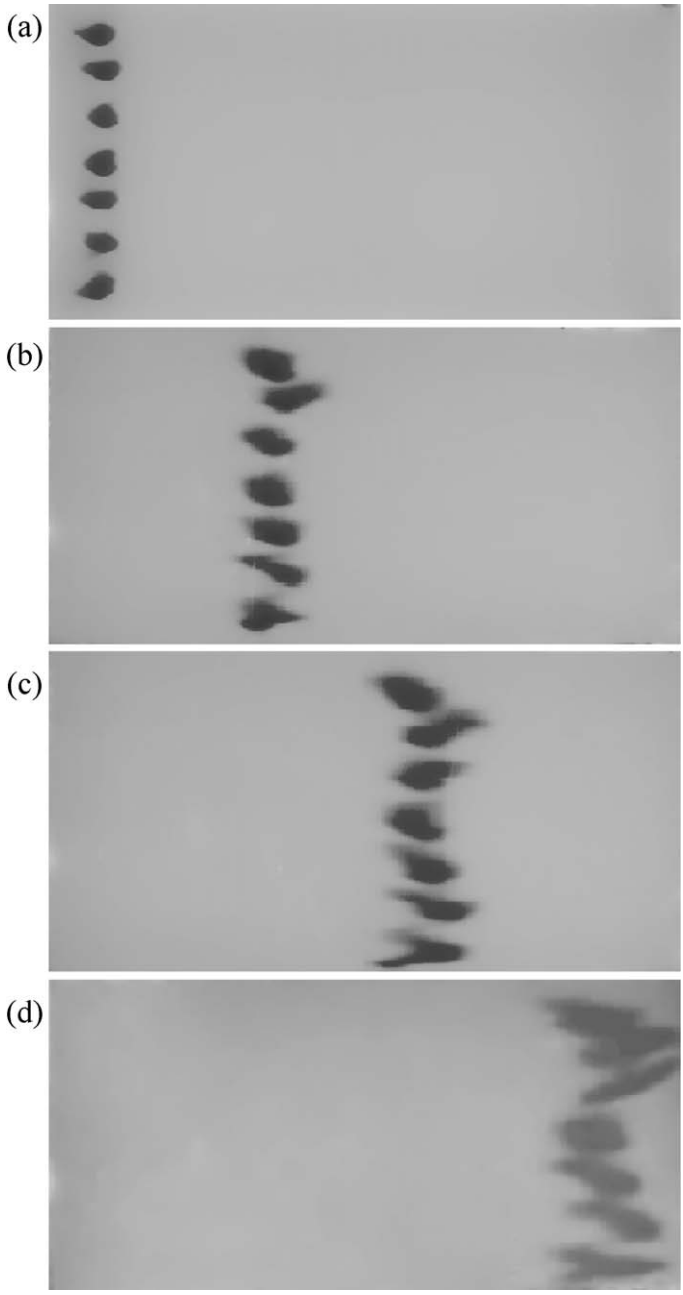

Fig. 7. Photographs of the homogeneous medium with seven dye tracer point injections being transported, under constant flow of 53 ml/min, from left to right. Times at (a) $t = 20$ min, (b) $t = 105$ min, (c) $t = 172$ min and (d) $t = 255$ min after injection.

one such experiment in the homogeneous medium, with a flow rate of 53 ml/min, taken at various time steps after pulse injection of dye. The dye was transported from left to right under mean uniform flow. Observe that the dye tracer plumes appear to be traveling more or less uniformly at early times. At later times, however, the tracer plumes become irregular in shape and appear to follow preferential pathlines, as shown in Fig. 7c,d.

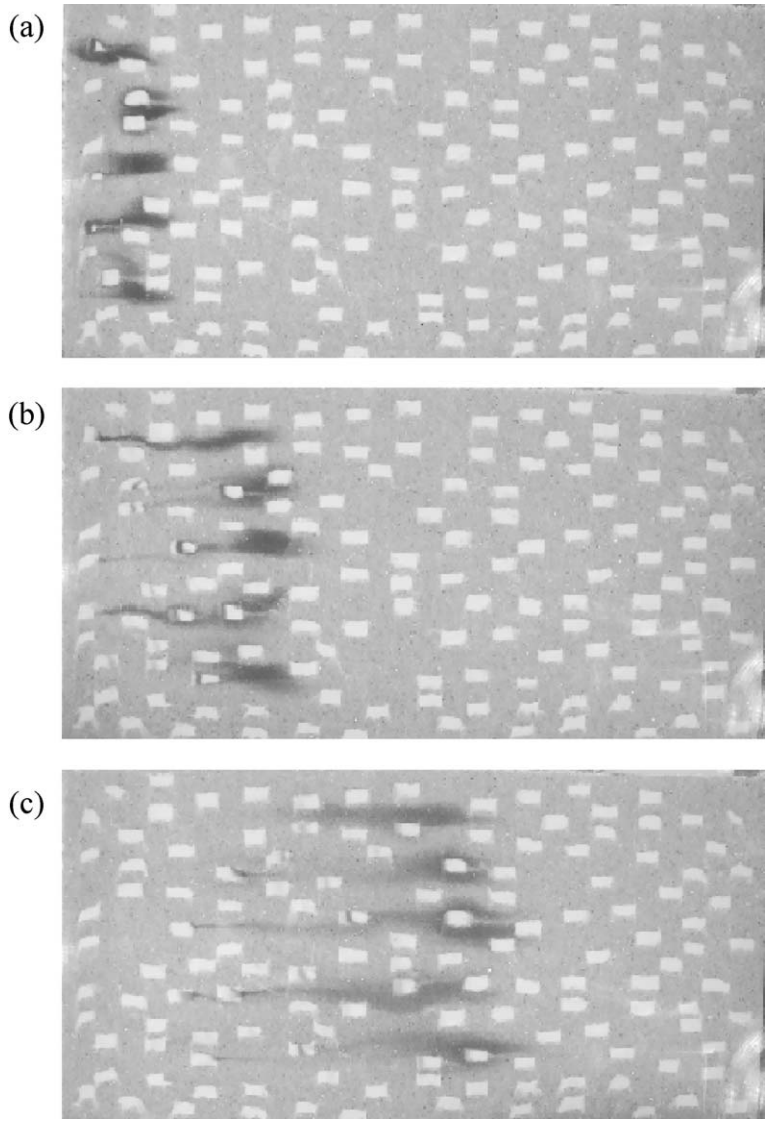

Fig. 8. Photographs of the randomly heterogeneous medium with five dye tracer point injections being transported, under constant flow of 65 ml/min, from left to right. Times at (a) $t = 16$ min, (b) $t = 49$ min and (c) $t = 115$ min after injection.

Similar observations were reported in homogeneous media using magnetic resonance imaging (e.g., Hoffman et al., 1996; Oswald et al., 1997). Therefore, it is not surprising that the ADE framework does not adequately describe the tracer breakthrough behavior at this flow rate. In heterogeneous systems, irregular behavior is noticed even at early times

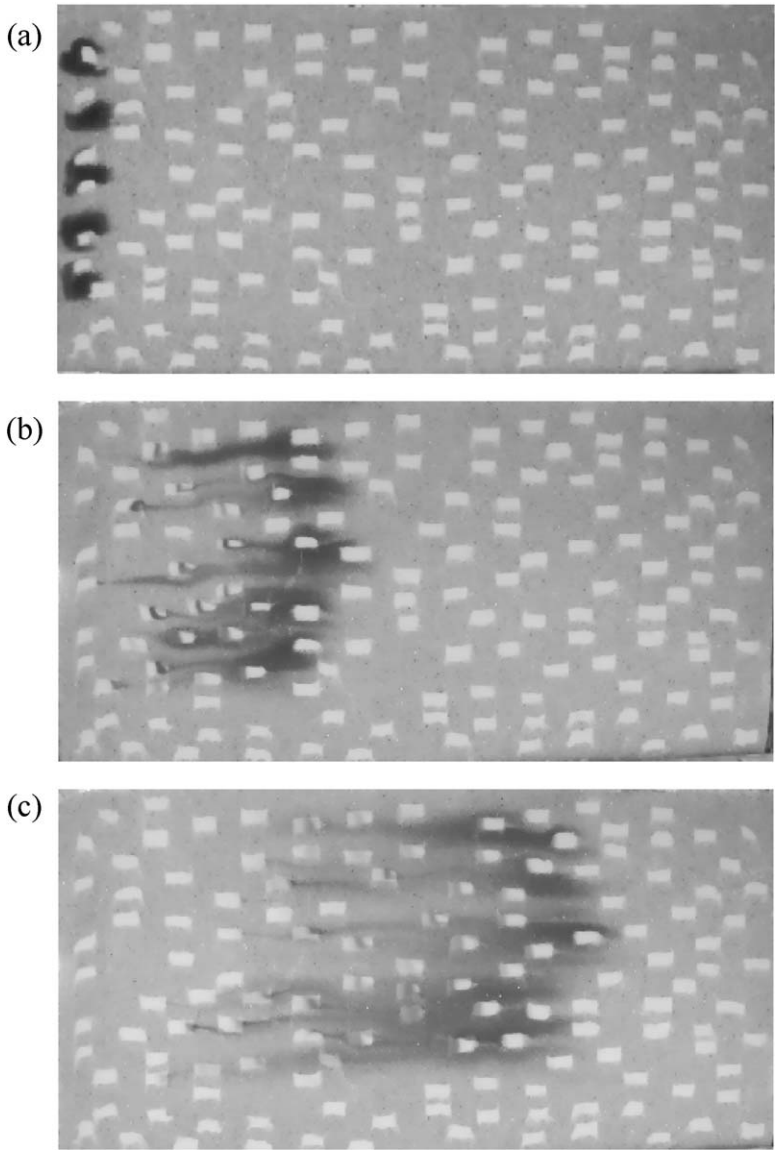

Fig. 9. Photographs of the randomly heterogeneous medium with five dye tracer point injections being transported, under constant flow of 35 ml/min, from left to right. Times at (a) $t = 13$ min, (b) $t = 156$ min and (c) $t = 317$ min after injection.

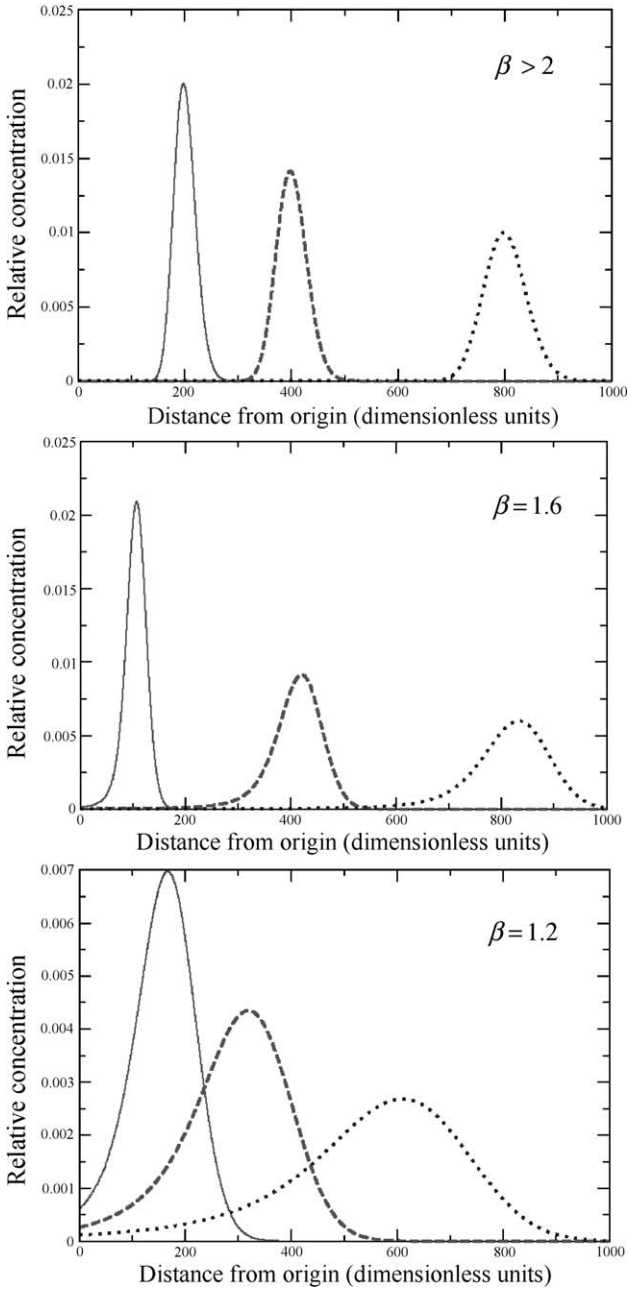

Fig. 10. Spatial profiles of tracer plumes at $\beta > 2$, $\beta = 1.6$ and $\beta = 1.2$. The solid, dashed and dotted curves in each plot represent early, intermediate and late dimensionless times.

as shown in Figs. 8 and 9. The large degree of non-uniform behavior visualized here is accounted for with lower β values in the CFPTD fits of the measured breakthrough data. Referring to Figs. 8 and 9, it is interesting to note the greater degree of spreading and smoothing in the slow flow rate experiment, which accounts for the higher β values in the breakthrough curves of the low flow rate experiments.

These dye tracer experiments are purely qualitative and for illustrative purposes only. If one "integrates" vertically across any of Figs. 7–9, to produce a spatial profile, Fickian or non-Fickian behavior can be discerned. More rigorously, analytical solutions of spatial profiles have been used to demonstrate that differences between Fickian and non-Fickian transport can be subtle, but important (Margolin and Berkowitz, 2002). Fig. 10 illustrates the temporal evolution of spatial profiles of a tracer injected as a pulse, for different values of β. For $\beta > 1$, the backward tails in the spatial plots, or the late time tails in the concentration versus time graphs, exhibit behavior that deviates most noticeably from Fickian behavior; differences between forward spatial tails, or early time tails, are less discernible. The shapes of these profiles can be compared qualitatively to the dye tracer experiments. Referring to Figs. 7–9, the plumes become more irregular as they travel through the porous media structures; the distinct backward tails become increasingly apparent, and depend on the packing structure and the flow rate of the given experiment. With this behavior in mind, compare, for example, the backward tail in Fig. 10b to the late time tail in Fig. 6c. Even at a β value of 1.6, which is approaching Fickian transport, the (non-Fickian) tails are still distinct and significant.

6. Concluding remarks

We have demonstrated that the CTRW framework is able to quantitatively capture a broad range of Fickian and non-Fickian transport behaviors. All measured breakthrough curves from the three sets of experiments are described by the CFPTD curves over the full range of flow rates investigated, whereas the classical advection–dispersion theory cannot effectively describe this behavior. In particular, the critical early and late time behaviors of the breakthrough curves are captured with the CTRW formulation. We emphasize that the characteristic information, which distinguishes non-Fickian transport from Fickian transport, lies precisely in these subtle yet measurable early and late arrival times. Many existing studies using the ADE report only "adequate" fits of breakthrough behavior due to deviation of data at the early and late times. Such differences become significant, for example, in analysis of issues related to groundwater remediation (particularly the late times) and escape of contaminants from subsurface waste repositories (particularly the early times).

We stress that the experimental set-up employed here permits study of the nature of the tracer transport. This is an important pre-requisite prior to testing the predictive capability of the model in natural geological settings. In nature, heterogeneity is ubiquitous; "homogeneous" formations do not exist. As clearly demonstrated here, tracer migration, even in "homogeneous" porous media, cannot always be described adequately by Fickian theory, thereby questioning the validity of transport theories using such assumptions. The CTRW theory quantitatively captures a broad range of Fickian and non-Fickian behavior

and thus demonstrates a practical and effective tool for the quantitative evaluation of contaminant transport in heterogeneous media.

Acknowledgements

We appreciate the assistance of Ran Kafri, Georg Kosakowski, Jason Levy and Steve Silliman, and thank Gennady Margolin for preparing Fig. 10. The financial support of the Israel Science Foundation is gratefully acknowledged.

References

Barth, G.R., Hill, M.C., Illangasekare, T.H., Rajaram, H., 2001. Predictive modeling of flow and transport in a two-dimensional intermediate-scale, heterogeneous porous medium. Water Resour. Res. 37 (10), 2503–2512.

Bear, J., 1972. Dynamics of Fluids in Porous Media. American Elsevier Publishing, New York.

Berkowitz, B., Scher, H., 1995. On characterization of anomalous dispersion in porous and fractured media. Water Resour. Res. 31 (6), 1461–1466.

Berkowitz, B., Scher, H., 1997. Anomalous transport in random fracture networks. Phys. Rev. Lett. 79 (20), 4038–4041.

Berkowitz, B., Scher, H., 1998. Theory of anomalous chemical transport in fracture networks. Phys. Rev., E 57 (5), 5858–5869.

Berkowitz, B., Scher, H., 2001. The role of probabilistic approaches to transport theory in heterogeneous media. Transp. Porous Media 42, 241–263.

Berkowitz, B., Scher, H., Silliman, S.E., 2000. Anomalous transport in laboratory-scale, heterogeneous porous media. Water Resour. Res. 36 (1), 149–158.

Berkowitz, B., Kosakowski, G., Margolin, G., Scher, H., 2001. Analysis of tracer test breakthrough curves in heterogeneous porous media using continuous time random walks. Ground Water 39 (4), 593–604.

Berkowitz, B., Klafter, J., Metzler, R., Scher, H., 2002. Physical pictures in heterogeneous media: advection–dispersion, random walk and fractional derivative formulations. Water Resour. Res. 38 (10), 1191.

Chao, H.C., Rajaram, H., 2000. Intermediate-scale experiments and numerical simulation of transport under radial flow in a two-dimensional heterogeneous porous medium. Water Resour. Res. 36 (10), 2869–2884.

Dentz, M., Berkowitz, B., 2003. Transport behavior of a passive solute in continuous time random walks and multirate mass transfer. Water Resour. Res. (in press).

Eggleston, J., Rojstaczer, S., 1998. Identification of large-scale hydraulic conductivity trends and the influence of trends on contaminant transport. Water Resour. Res. 34 (9), 2155–2168.

Garabedian, S.P., LeBlanc, D.R., Gelhar, L.W., Celia, M.A., 1991. Large-scale natural gradient tracer test in sand and gravel, Cape Cod, Massachusetts: 2. Analysis of spatial moments for a nonreactive tracer. Water Resour. Res. 27 (5), 911–924.

Gelhar, L.W., Welty, C., Rehfeldt, K.R., 1992. A critical review of data on field-scale dispersion in aquifers. Water Resour. Res. 28 (7), 1955–1974.

Glass, R.J., Steenhuis, T.S., Parlange, J.-Y., 1988. Wetting front instability as a rapid and far-reaching hydrologic process in the vadose zone. J. Contam. Hydrol. 3, 207–226.

Hatano, Y., Hatano, N., 1998. Dispersive transport of ions in column experiments: an explanation of long-tailed profiles. Water Resour. Res. 34 (5), 1027–1033.

Hoffman, F., Ronen, D., Pearl, Z., 1996. Evaluation of flow characteristics of a sand column using magnetic resonance imaging. J. Contam. Hydrol. 22, 95–107.

Kosakowski, G., Berkowitz, B., Scher, H., 2001. Analysis of field observations of tracer transport in a fractured till. J. Contam. Hydrol. 47, 29–51.

Margolin, G., Berkowitz, B., 2000. Application of continuous time random walks to transport in porous media. J. Phys. Chem., B 104 (16), 3942–3947 (Correction: J. Phys. Chem., B 104 (36) (2000) 8762).

Margolin, G., Berkowitz, B., 2002. Spatial behavior of anomalous transport. Phys. Rev., E 65, 1–11 (031101).

Oswald, S., Kinzelbach, W., Greiner, A., Brix, G., 1997. Observation of flow and transport processes in artificial porous media via magnetic resonance imaging in three dimensions. Geoderma 80, 417–429.

Scher, H., Lax, M., 1973a. Stochastic transport in a disordered solid: I. Theory. Phys. Rev., B 7 (10), 4491–4502.

Scher, H., Lax, M., 1973b. Stochastic transport in a disordered solid: II. Impurity conduction. Phys. Rev., B 7 (10), 4502–4519.

Schincariol, R.A., Schwartz, F.W., 1990. An experimental investigation of variable density flow and mixing in homogeneous and heterogeneous media. Water Resour. Res. 26 (10), 2317–2329.

Schroth, M.H., Ahearn, S.J., Selker, J.S., Istok, J.D., 1996. Characterization of Miller-similar silica sands for laboratory hydrologic studies. Soil Sci. Soc. Am. J. 60, 1331–1339.

Silliman, S.E., Caswell, S., 1998. Observations of measured hydraulic conductivity in two artificial, confined aquifers with boundaries. Water Resour. Res. 34 (9), 2203–2213.

Silliman, S.E., Simpson, E.S., 1987. Laboratory evidence of the scale effect in dispersion of solutes in porous media. Water Resour. Res. 23 (8), 1667–1673.

Silliman, S.E., Wright, A.L., 1991. Generation of random fields characterized by discrete regions of constant value. Appl. Math. Comput. 45, 293–311.

Silliman, S.E., Zheng, L., Conwell, P., 1998. The use of laboratory experiments for the study of conservative solute transport in heterogeneous porous media. Hydrogeol. J. 6, 166–177.